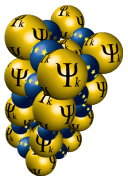

Ψ_k **Scientific Highlight Of The Month**

No. 148 **March 2020**

Questaal: Electronic structure for the future

Dimitar Pashov[1], Swagata Acharya[1], Jerome Jackson[2,*], Brian Cunningham[3], Myrta Grüning[3], Mark van Schilfgaarde[1]

[1] *Department of Physics, King's College London, Strand, London WC2R 2LS, United Kingdom*
[2] *Scientific Computing Department, STFC Daresbury Laboratory, Warrington WA4 4AD, United Kingdom*
[3] *School of Mathematics and Physics, Queens University Belfast, Belfast BT7 1NN, Northern Ireland, United Kingdom*

Abstract

We report on progress in the Questaal, a CCP9 flagship electronic structure package written for electronic structure methods of the future. Questaal has a density-functional implementation with many features similar to other large scale packages, but its unique features are in its implementation of Green's function methods. Questaal has a two-track implementation of Green's functions: through many-body perturbation theory and through Dynamical Mean Field theory. The first path is based on the Quasiparticle Self-Consistent GW (QSGW) approximation. This is important because QSGW does not rely on DFT, which dramatically improves on the quality and reliability of MBPT. We show how, in contrast to DFT-based GW, QSGW predicts one-particle properties such as energy band structures, and two-particle properties such as susceptibilities, in a consistent and uniform manner, provided spin fluctuations are not strong. DMFT provides the essential additions to QSGW to handle spin fluctuations. We show how extensions to QSGW can provide a high-fidelity description of both one-and two particle properties for a remarkably wide range of properties and materials systems. We show how some extensions of QSGW+DMFT provides a promising path for *ab initio* description of unconventional superconductivity.

Questaal is a suite of several codes. One is a layer code, based in density functional theory, that implements non-equilibrium transport in Landauer-Buttiker approximation. Some novel features and applications are outlined. There is also emerging a new functionality, phonons and the electron-phonon interaction based on MBPT. This represents a significant advance over the usual DFPT approach.

This Psi-k highlight is the abridged version of an article published in Computer Physics Communications, Volume 249, Dimitar Pashov, Swagata Acharya et al., *"Questaal: A package of electronic structure methods based on the linear muffin-tin orbital technique"*, 107065, Copyright Elsevier 2020 (under a Creative Commons license).

*jerome.jackson@stfc.ac.uk

1 Introduction

This highlight summarises some features of Questaal as it is currently implemented[1], and it also points to new developments that will soon become operational, in particular a new basis set, advances in predicting properties of unconventional superconductors, and modelling of spin-torque and JMRAM devices. While its present form as a CCP9 community code is fairly recent, Questaal is a long established code. It got its start in the 1980's, in O.K. Andersen's group in Stuttgart. Andersen, who formulated the modern theory of linear band methods, developed a standard package based on the LMTO-Atomic Spheres approximation. It has evolved a great deal since then, with many innovations have been built into Questaal and its antecedents. It was one of the first noncollinear magnetic codes and the original *ab initio* description of spin dynamics was implemented in it, as were the first calculations of electron-phonon interaction for superconductivity, of instanton dynamics, of impact ionisation, of exact exchange and exact exchange+correlation; the first GW implementation based on an all-electron method, and extensions to include spin fluctuations through Dynamical Mean Field Theory, and an early density-functional implementation of nonequilibrium Green's functions for Landauer-Buttiker transport. Questaal is a community code which descended from these prior developments – details about the project can be found in a recent review [1].

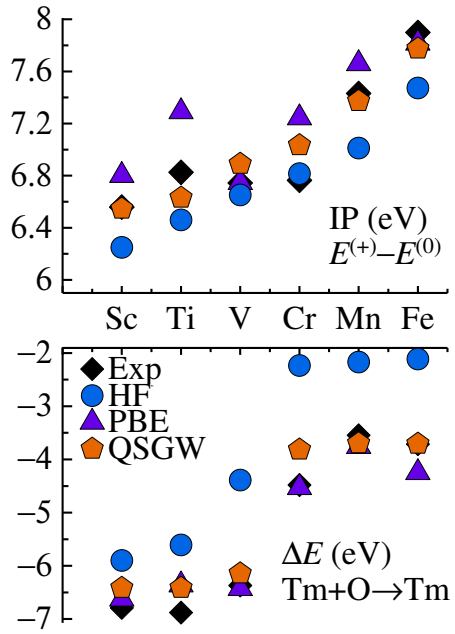

Figure 1 – (top) Ionisation potential, IP, of TM atom and (bottom) heat of formation ΔE of transition-metal dimers computed within the Random Phase approximation,selecting various choices of starting point. Note the dramatic difference between Hartree-Fock and PBE starting points. Of the common semi-empirical functionals, HSE06 (not shown) is the closest to QSGW. In QSGW errors are slightly larger than "quantum chemical" accuracy which can be achieved with high-level quantum-chemical methods for small molecules. Data were compared to reference CCSD(T) for the ionisation potential and experiment for ΔE.

2 Present Status

Present-generation advanced electronic structure codes for solids are grounded almost entirely on DFT and many-body methods that extend a DFT starting point (DFT^{++}). But because DFT, in practice, depends on an uncontrollable ansatz, such a model is ill-suited as a foundation for realising the fully predictive paradigm of the future. Our vision is to create a scalable software package fully constructed around a Green's function framework, without reliance on DFT or extensions to it, capable of accurately predicting an intrinsically diverse range of static and dynamical materials phenomena in an integrated and hierarchical manner. Creating such a code offers a completely fresh approach to the many-body problem, one that starts from a point far superior to DFT, and moreover, one that can be systematically improved. It is much better positioned to achieve the prescriptive design of functional materials, because as successful as DFT is, extensions to improve on it cannot be systematic. The result is inevitably a patchwork quilt of extensions, as is found today.

The twin features of most established codes (planewave basis, and density functional theory) that have contributed so much to the success of electronic structure theory, and still do, will eventually constrain the power and reach that more powerful Green's function methods can offer in these codes. A testament to the success of DFT is its widespread adoption and extensions through a plethora of specialised strategies and patchwork of extensions that, e.g., correct quasiparticle levels or level alignments, incorporate dispersion forces, improve reaction energies, improve the charge density or magnetic properties, or include dynamical fluctuations to handle strong correla-

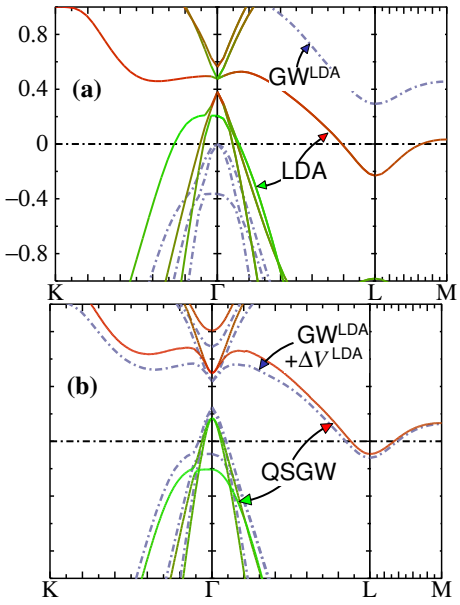

Figure 2 – Energy bands in $TiSe_2$ (in eV), for the undistorted $P\bar{3}c1$ structure. (a): solid lines are LDA results, with red and green depicting a projection onto Ti and Se orbital character, respectively. Blue dashed line shows shifts calculated in the GW approximation based on the LDA. (b): blue dashed line shows results from GW based on the LDA (same self-energy as in panel (a)), with an extra potential $\Delta V^{\rm LDA}$ deriving from a charge density shift computed from the rotation of the LDA eigenvectors. Solid lines are QSGW results, with the same colour scheme as in panel (a).

tions. However, it is increasingly recognised that unsystematic and uncontrollable errors inherent in DFT ultimately limit what such a strategy can do. The adverse consequences are well known to DFT^{++} practitioners; they are especially apparent when materials are correlated or chemically heterogeneous.

Figs. 1 and 2 adopt two examples from Ref. [1] to illustrate this point. Ambiguities in the starting point (selection of one-body Hamiltonian used to make, e.g. GW) make it difficult to know what errors are intrinsic to the theory and which are accidental. The literature is rife with manifestations of this problem; see e.g. Ref. [2]. Fig. 1 shows the ionisation potential of 3d transition metal atoms and the heat of formation of 3d-O dimers,* computed by the `molgw` code [4]. Note how results depend sensitively on whether the one-body Hamiltonian generating W or GW is based on PBE or Hartree Fock. Quasiparticle self-consistency[5, 6, 7] largely removes the ambiguity so that the errors intrinsic to the GW approximation can be best elucidated. It should moreover, yield better RPA total energies on average than those calculated from other starting points, because the path of adiabatic connection is optimally described [7]. With the exception of Cr (an outlier because of strong spin fluctuations; see §6), results in the Figure largely support this argument.

Fig. 2 shows the energy band structure of $TiSe_2$, a layered diselenide with space group $P\bar{3}m1$. Below T_c=200K, it undergoes a phase transition to a charge density wave, forming a commensurate 2×2×2 superlattice ($P\bar{3}c1$) of the original structure. It is well known that LDA-based GW has a tendency to slightly underestimate the gap which can be problematic in narrow-gap systems†. $TiSe_2$ is an unusual case because GW based on LDA significantly *overestimates* the band gap. Self-consistency significantly modifies the Hartree potential, which reduces the gap; and so $TiSe_2$ suffers from the opposite problem than is usual. This correction turns out to be a common feature in polar compounds generally (see e.g. Fig. 3 in Ref. [6]), but the gap is small in $TiSe_2$ so the difficulty is more easily uncovered.

Finally, self-consistency is essential for any proper description of magnetism: local moments that form are sensitive to it. For an example, see the discussion of VO_2 in §5.

A corollary to the success of DFT^{++} is the pervasive use of planewave (PW) basis sets for implementation, because they can be systematically converged. However, it has long been known that many-body effects in a PW basis are painfully slow to converge, and the difficulty becomes increasingly acute the stronger the correlations (which are naturally localised). Even with leadership-class computing resources, severe computational demands limit the scope of accessible properties. This results in a multiplicity of strategies to truncate, interpolate, transform, approximate, or otherwise avoid the problem of

*We focus on these properties because it is known, e.g. from Ref. [3], that the RPA tends to systematically overbind, and the error is connected with short-ranged correlations. The ionisation potential and the dimer formation energy, both of which benefit from partial cancellation of such errors, are much better described.

†$G^{\rm LDA}W^{\rm LDA}$ is often problematic when LDA inverts the gap; for example in PbTe the L_6^+ and L_6^- are inverted (see Fig. 13 of Ref. [1]). When GW is added to LDA perturbatively, the ordering at L is corrected, but the inversion in the gap cannot be topologically disentangled since off-diagonal parts of the self-energy are omitted. This problem occurs in many narrow-gap semiconductors. Ge is another example; see Fig. 5 of Ref. [8].

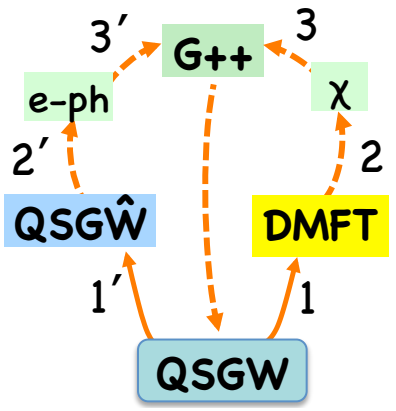

Figure 3 – Questaal strategy for solving the many-electron problem. For systems with weak spin fluctuations, low-order extensions QSGW yield uniformly accurate electronic structure (left track). Materials with strong spin fluctuations usually require a nonperturbative approach (right track). Either can generate G, which is needed to predict derived functional properties (G^{++}). These properties can feed back at a higher level of theory and improve G (vertical dashed line).

slow convergence[9, 10, 11, 12, 13]. This suggests that the most successful scalable electronic structure codes of the future will not be using a PW basis for many-body methods. Taken together with the unsystematic character of DFT, methods that employ a rapidly converging nearsighted basis and algorithms that do not depend on DFT can provide an ideal and uniquely capable computational platform upon which to build the electronic code of the future.

3 Questaal's promise

Questaal, with a new compact real-space basis of Jigsaw Puzzle Orbitals to be described below, offers a very promising—perhaps the most promising—path to surmount these limits without sacrificing precision. The best beyond-DFT methods start from the GW approximation and then divide mostly into two "flavors": nonlocal but low-order many-body perturbation theory, and nonperturbative but local approaches (Fig. 3). These two tracks approximately coincide with actual functional materials. Those with strong spin fluctuations are best suited to the right track (Fig. 3) and those without strong spin fluctuations to the left track. This assertion is mostly (but not strictly) true, and it is largely because the effective interaction governing spin fluctuations is mostly local, whereas the coulomb interaction is long ranged; but fortunately, low-order theory appears to work very well. Sec. 5 and 6 provide some benchmarks to support these assertions.

With a high-fidelity G in hand, functional materials properties, such as total energy, spin susceptibility, or superconducting gap functions, can be reliably derived (G^{++} in Fig. 3). Finally, some of these derivative properties can feed back to G to include higher-level diagrams and can systematically improve it. In special cases, additional refinements to G are needed. One such example is the low-temperature nematic (orthorhombic) phase in FeSe: neither QSGW nor QSGW+DMFT seems to adequately describe *nonlocal* spin fluctuations need to fully discriminate between the a and b axes. Fig. 3 epitomises Questaal's hierarchical approach. Work is in progress to add diagrams to the self-energy not included in the RPA. One operational example is the addition of ladder diagrams to W; another is the addition of electron-phonon diagrams in a MBPT framework.

4 Jigsaw Puzzle Orbitals

The basis set forms the core of any method that solves the Schrödinger equation. Questaal is an all-electron, augmented wave method. At present its envelope functions are convolutions of Hankel functions and Gaussian functions — generalisations of standard LMTO's that give them more flexibility and accuracy. Also, if needed, plane waves can be added to the envelope functions (APWs) [14].

Ideally, a basis set should be *complete*,*minimal*, and *short ranged*, and while the existing basis are reasonably complete, they do not meet these requirements. A new basis set that we have dubbed Jigsaw Puzzle Orbitals will have a unique ability to largely meet these requirements *simultaneously*, in an optimal manner. It does so by extrapolating accurate solutions of Schrödinger's equation computed numerically inside the augmentation spheres, to construct optimal envelope functions that link nuclei together. All atom-centred methods do this, but JPOs are unique in that the envelope functions are constructed in a (nearly) optimal manner by solving local Green's function around an atom, subject to special-purpose boundary conditions designed to construct envelope functions which make the kinetic energy continuous everywhere.

The Schrödinger equation is carried entirely by a single partial wave close to any augmentation sphere, uncontaminated by other partial waves. By construction, the JPO basis is thus nearly optimal. The only errors for a given potential are those in interpolation between augmentation spheres, and the usual energy linearisation error. Basis functions have exact Slater-Koster form on the augmentation sphere boundary (Fig. 4): so they bear some resemblance to atomic orbitals, but they are shorter ranged.

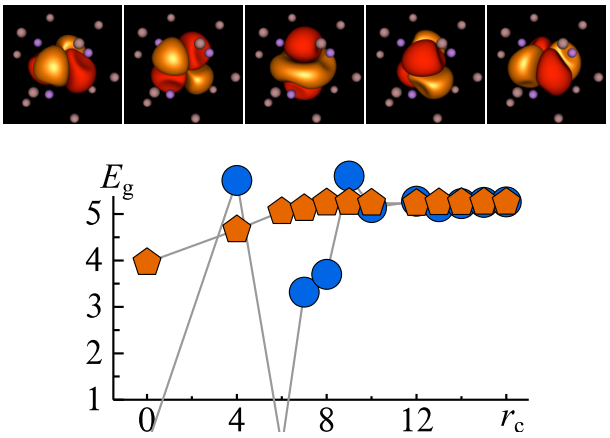

Figure 4 – Screened d envelope functions, xy, yz, $3z^2-1$, xz, and x^2-y^2, for a zincblende lattice. Bottom: Bandgap in NiO as a function of the cutoff $|\mathbf{R}'-\mathbf{R}|$ in the QSGW self-energy $\Sigma^0_{\mathbf{RR}'}$ for traditional envelope functions (blue) and screened basis set (orange). The first point contains onsite terms only, the second adds first neighbours etc. The conventional basis shows erratic behaviour until at least the fourth neighbours are present.

To date, we have succeeded in constructing "screened" versions of Questaals basis functions (convolutions of Gaussian and Hankel functions). Screening is reminiscent of Andersen's tight-binding transformation[15] of traditional LMTOs[16] and yields short-ranged functions. At this stage the basis set is short-ranged unitary transformation of the existing Questaal basis: short range and good quality but not optimal. When modified to make the kinetic energy continuous everywhere, their quality should improve significantly and yield well converged calculations similar to LAPW. These "Jigsaw Puzzle Orbitals" are tangentially related to Andersens NMTO method[17] but they are more general, more accurate, shorter ranged, and suited for modern full-potential methods. Even while NMTO are ill suited to modern methods, they demonstrate how the quality of traditional LMTO basis sets can be dramatically improved. They provide proof-of principle, and give us confidence that JPOs will be very accurate over the relevant energy window (in a linear approximation, roughly $E_F \pm 1\,\mathrm{Ry}$).

5 Illustrations of QSGW

Questaal is framed on a hierarchical strategy around the premise that low-order MBPT well describes the vast majority of cases where spin fluctuations are not strong (Fig. 3). At the lowest level is QSGW, which depends only minimally on DFT. That it does not rely on DFT is central importance to frame a consistently reliable theory, for reasons we have pointed out in Sec. 2 and in Ref. [1].

A fair body of experience shows that QSGW is adequate for many purposes. Note for example the stellar agreement with ARPES in elemental Fe, and the Fermi surface in Sr_2RuO_4 in Fig. 5. Often though, errors appear. Usually they are small and systematic, and can be traced to a missing diagram. In such a case the present implementation of Questaal has two routes to improve on G. The first is a perturbative, nonlocal path ($1', 2', 3'$ in Fig. 3), where low-order diagrams are added to W to make ($W \to \widehat{W}$). When doing so for a wide range of insulators, fundamental gaps are in excellent agreement with experiment (see panel (b) in Fig. 5).

Quantities related to the two particle properties, spin and charge susceptibilities, are the primary observables in spectroscopies. In the MBPT context some instances of the dielectric function are shown in Fig. 5, and the first paper on spin waves based on QSGW yields very good descriptions in NiO, MnO, and MnAs [18]. Going beyond RPA was essential for VO_2, and La_2CuO_4. In the La_2CuO_4 case it is necessary to include ladders not only in the response function but also in the QSGW cycle ($W \to \hat{W}$ in Fig. 3). Self-consistency is necessary to get good agreement such as shown in Fig. 5 and Ref. [18].

To date we have added ladders to the charge channel, but other additions can be included in this path. Savio Laricchia is nearing completion of a project to add the electron-phonon interaction perturbatively [19], thus adding another bosonic contribution to W. He has shown, for example, that provided ladders are included in W, he can obtain very good descriptions of the

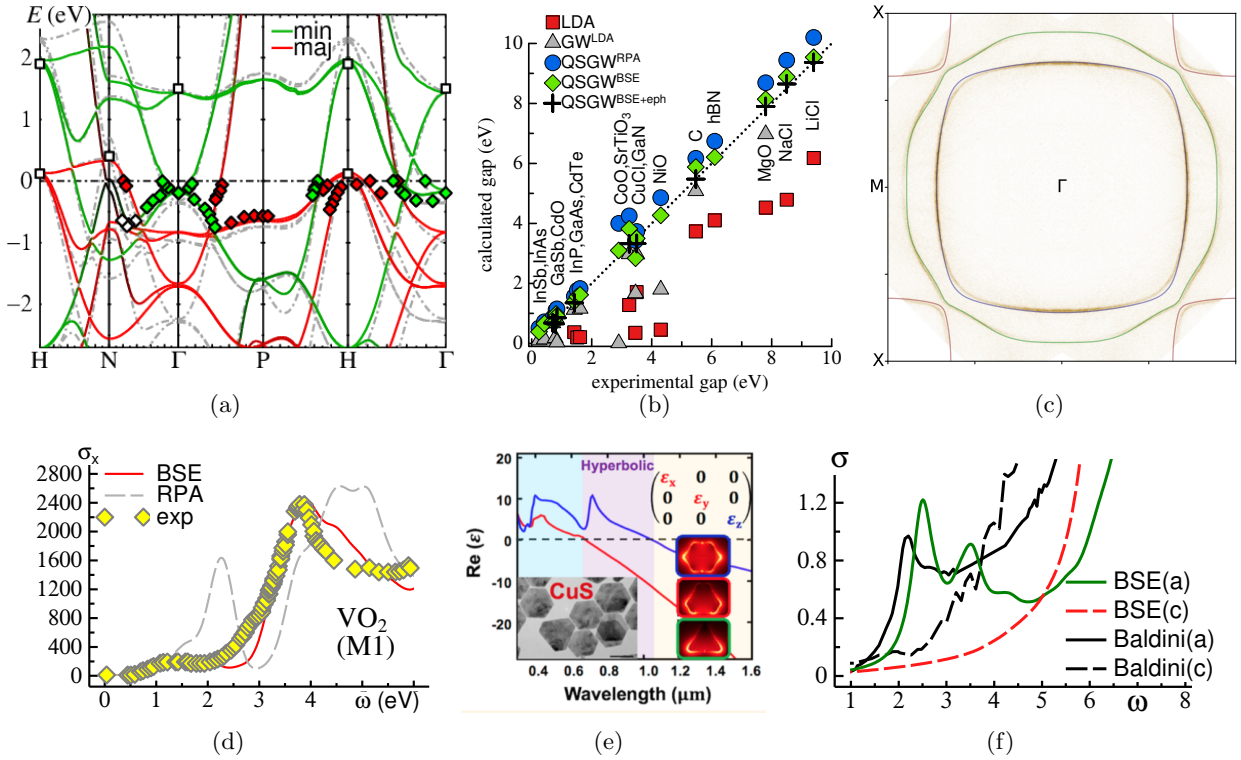

Figure 5 – Top row refers to 1-particle properties, illustrating the fidelity of the QSGW electronic structure in cases when spin fluctuations are not strong. **(a)** QSGW band structure of Fe (solid lines), LSDA (grey dashed), ARPES spectra (diamonds) and inverse photoemission spectra (squares). **(b)** Right: Bandgaps in selected insulators, comparing Local Density Approximation (LDA), $G^{\rm LDA}W^{\rm LDA}$, QS$GW^{\rm RPA}$, QS$GW^{\rm BSE}$, with and without an approximate phonon correction from $\Sigma^{\rm e\text{-}ph}$. **(c)** ARPES and QSGW Fermi surface of Sr_2RuO_4. Slight discrepancies can be observed. Bottom row shows optical conductivity or dielectric function for three correlated materials. Generally agreement is excellent. **(d)** RPA, BSE, and experimental conductivity in VO_2. **(e)** Real part of the dielectric function in CuS along the a and c axis, showing regions of dielectric (blue), hyperbolic (pink) and plasmonic (yellow) optical response. **(f)** Experimental (black) and BSE (red, green) conductivity in La_2CuO_4 along the a and c axis. Discrepancies at higher ω in La_2CuO_4, are thought to originate from spin fluctuations missing in QSGW. Figures are taken from Ref. [20] (panel a), a paper in preparation by the authors of Ref. [21] (panels b and f); Ref. [22] (panel c); Ref. [23] (panel d); Ref. [24] (panel e). Measurements in panel f are taken from Ref. [25].

phonon contribution to the quasiparticle levels in diamond and graphene (this will be reported elsewhere).

Also possible, but not yet accomplished within Questaal, is to add low order spin fluctuation diagrams such as the T matrix [26]. All of these diagrams improve the self-energy and make a better G (G^{++} in Fig. 3).

As for the spin susceptibility, low order MBPT can provide good results when spin fluctuations are not large, as occurs in local moment systems such as NiO and MnAs. But low order MBPT is not suitable for the more interesting cases where spin fluctuations are important, as the next section describes.

6 QSGW+DMFT

In all of the cases discussed so far (except La_2CuO_4 to some extent), spin fluctuations are weak. As they become strong, as they do in many unconventional superconductors and other strongly correlated materials, the description of one-particle and two-particle properties by QSGW begins to break down. Often such materials are "bad metals" with a significant amount of incoherence in spectral functions even at the Fermi level. Augmenting MBPT with DMFT can be essential here. The spin susceptibility χ^s via DMFT is vastly better than computing it by low-order MBPT such as T matrix. For one, proper treatment the full three-frequency dependent vertex (two fermionic frequencies and one bosonic frequency) can be very important. This is not done in practice with T matrices because of the prohibitive cost. Secondly, magnetic energies are small (on the order of k_BT), leading to competition between many kinds of electronic configurations of similar low energy. This can be seen already at the DFT level [27]. Thirdly, because of multiple competing effects on a low energy scale, χ^s can be sensitive to temperature, and indeed we find this to be the case in systems such as $Sr_xLa_{2-x}CuO_4$.

All of this motivates the second path (right path, Fig. 3). It begins (1) as a construction of a nonperturbative but local G, implemented by augmenting QSGW with Dynamical Mean Field theory (DMFT). DMFT generates a local but frequency- and temperature- dependent self-energy. It handles local correlations very well but it misses nonlocal correlations. In the Questaal framework DMFT is built on top of QSGW instead of DFT, and nonlocality is built into the bath H_0. Neither DFT and DMFT have nonlocality, but it can be important: note, for example the orbital- and k-dependence of the Z factor in FeSe, Fig. 6. DMFT adds another (k independent) renormalisation to Z on top of QSGW, and it has been argued [28, 29] that the nonlocal correction supplied by QSGW is important for a proper description of the spectral function generated by DMFT. In Ref. [28], Tomczak presented some evidence that for Fe superconductors in the Fermi liquid regime, $\Sigma(k,\omega)$ can be well approximated by a separable form, $\Sigma_1(k)+\Sigma_2(\omega)$.

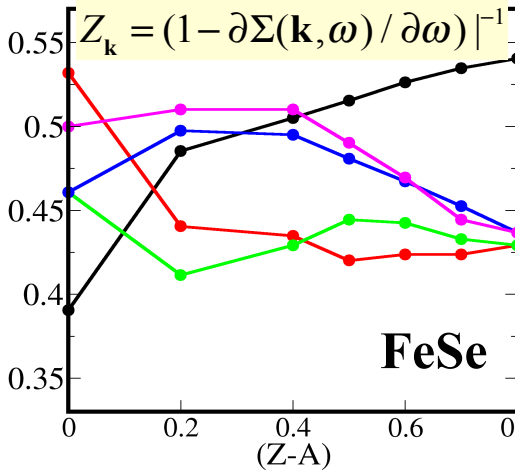

Figure 6 – k dependent Z factor in the tetragonal phase of FeSe, on the Z-A line, for the five d bands. Z is computed from QSGW. Z is defined by the formula in the figure. DMFT makes a further reduction of Z, but the DMFT contribution to Z is k-independent.

Fig. 5 shows how the charge contribution to Σ seems to be very well described by QSGW (or QS$G\hat{W}$). It is widely thought that the interaction kernel entering into the *magnetic* diagrams is largely confined to a region centred around a nucleus where the local moment is not negligible. In DFT this is strictly true. The DFT analogue, $f_{xc} = \partial^2 E/\partial\mathbf{m}\partial\mathbf{m}$, is taken to be strictly local. Thus to a good approximation the magnetic contribution to the potential is site-local, which DMFT is designed to calculate with high fidelity[‡]. If moreover the cross coupling between the magnetic and charge channels is small, approximating the full self-energy Σ with a sum of

[‡]This argument is a little misleading. The constituents of a local self-energy can originate from nonlocal diagrams. Nevertheless it is mostly true that the great magnetic contribution to the local self-energy almost entirely originates from local diagrams.

charge and spin diagrams

$$\Sigma(k,\omega) \approx \Sigma^c(k,\omega) + \Sigma^m(\omega)$$

is a good approximation. The cross-coupling is usually small because their energy scales are so different. A typical plasmon energy is in excess of 1 eV, and and a typical magnon energy typically ranges between a few and a few hundred meV.

Moreover QSGW (or QS$G\hat{W}$) appears to do an excellent job describing $\Sigma^c(k,\omega)$. DMFT adds a k independent contribution to Σ^c, but in the QSGW+DMFT context, its primary importance lies in its contribution to $\Sigma^m(\omega)$. DMFT is well suited to well capture most spin phenomena, as it is an explicitly temperature dependent theory that includes all local graphs.

There are some exceptions where this partitioning breaks down: the nematic phase of FeSe and the pseudogap phase of $Sr_xLa_{2-x}CuO_4$ are two instances where k dependent spin diagrams are needed to reliably capture the phenomena. But for the great majority of cases, QSGW+DMFT does an excellent job in its prediction of one particle properties. It correctly describes the metal-insulator transition in La_2CuO_4 induced by excited phonons, and it accurately distinguishes which phonons can bring it about (Ref. [25]).

The material that perhaps most convincingly demonstrates separate roles of spin and charge is VO_2. At high temperature VO_2 is monoclinic (M_1 phase), which is insulating in contrast to the rutile phase observed at low temperature. While there has been a fair amount of debate about the origins of the gap, evidence from GW theory [30, 23] shows rather convincingly that M_1 VO_2 is a band insulator. The unit cell of M_1 has four V atoms, which dimerise into two V-V pairs. There is also a metastable M_2 phase, closely related to the M_1 but in M_2 only one of the two V pairs dimerise. A QSGW calculation of the M_1 phase[23] yields a band insulator, similar to what Gatti and coworkers found [30], and predicts the system is nonmagnetic. A nonmagnetic QSGW calculation of VO_2 in the M_2 phase, however predicts it to be a metal, in contradiction to experiment. If allowed to form local moments, it is found that moments vanish on the dimerised pair, as in the M_1 phase, but appear on the undimerised pair. These moments are antiferromagnetically aligned, and they cause a gap to form, much as occurs in other antiferromagnetic insulators such as CoO and La_2FeO_4. Above room temperature where the M_2 phase is observed, VO_2 is very likely paramagnetic. Thus we expect the gap to form in M_2 only because of fluctuating local magnetic moments, while in M_1 it is an ordinary band insulator.

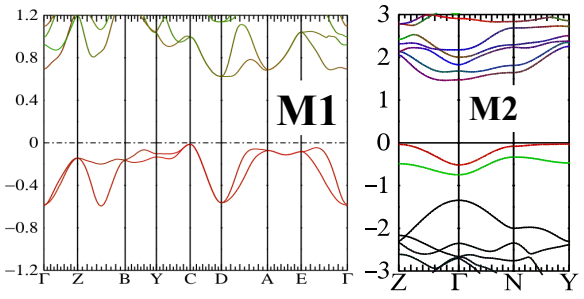

Figure 7 – (left) Energy band structure of VO_2 in the M_1 phase, computed by QSGW. The calculation predicts no local moment. (right) Corresponding calculation for the M_1 phase. The undimerised V-V pair is predicted to order antiferromagnetically, with a local moment of $0.7\mu_B$, while the dimerised pair is predicted to have no moment.

DMFT can also be used to make the local two-particle Green's function. This provides a local vertex, which when combined with nonlocal bubbles $G\otimes G$, yields charge and spin susceptibilities that depend on both k and ω (point (2) in Fig. 3). In the cases where we can compare to reliable measurements of spin susceptibility (FeSe, Sr_2RuO_4, $Sr_xLa_{2-x}CuO_4$, YBCO, YFe_2Ge_2) we generally find very good agreement. The strong temperature dependence in χ^s sometimes observed could be confirmed by neutron experiments, for example. This can be very important: calculations of χ^s for $Sr_xLa_{2-x}CuO_4$ show that it vanishes at $\omega = 0$ below 145 K at the all-important (π,π) point. This has a pronounced effect on the superconductivity.

Susceptibilities can be combined to yield other quantities, most notably an estimate for superconducting gap function (see Ref. [22]) and superconducting critical temperature. We have studied several materials systems, and the results are remarkably good in cases we have studied so far, e.g. in Sr_2RuO_4, Ref. [22]. Fig. 32 of Ref. [1] is reproduced here in Fig. 8.

The theory is still new and it misses some effects in its present form: for example it does not distinguish competing phases like the antiferromagnetic phase. Still, developing an ability to reliably derive superconducting quantities *ab initio* will provide a path to a proper understanding of unconventional superconductivity that was not possible before, and it will also discriminate

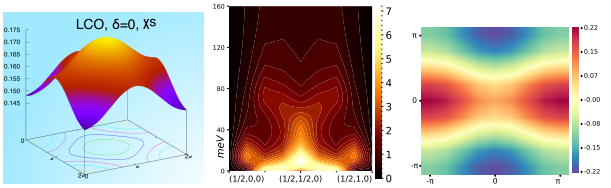

Figure 8 – (left) Real part of $\chi^s(q,\omega{=}0)$ for La_2CuO_4 showing a dominant peak at $\mathbf{q}{=}(\pi,\pi)$. (middle) Imaginary part of $\chi(q,\omega)$ (arbitrary units) for $La_{1.88}Sr_{0.12}CuO_4$ showing that spin fluctuations get gapped at (π,π) below 145 K. (right) Nodal superconducting gap structure for the hole-doped La_2CuO_4 showing $d_{x^2-y^2}$ gap symmetry. The colour bar shows the negative (in blue) and positive (in red) superconducting gap magnitudes in arbitrary units passing through node where the gap closes (in yellow). Taken from Ref. [1].

between competing mechanisms. We at least partially demonstrated this in Sr_2RuO_4, a particularly difficult case. An adequately developed theory will constitute an enormous advance in the field.

7 Applications of the Layer Green's function technique

Questaal also has two density-functional based Green's function codes, a crystal code that has been used primarily to calculate magnetic exchange interactions through the classic Lichtenstein formula [31], and a layer Green's function technique that has periodic boundary conditions in only two dimensions. Along the third dimension it has a trilayer form: an active region cladded on each end by semi-infinite leads.

$$\overbrace{\ldots \mathrm{PL}\ -1}^{\mathrm{PLATL}} \;\Big|\; \overbrace{\mathrm{PL}\ 0 \,|\, \ldots \,|\, \mathrm{PL}\ n{-}1}^{\mathrm{PLAT}} \;\Big|\; \overbrace{\mathrm{PL}\ n\ \ldots}^{\mathrm{PLATR}}$$

Provided the Hamiltonian is short-ranged the principal layers can be constructed so the Hamiltonian matrix elements extend only to neighbours. This makes the Hamiltonian tridiagonal in the PL index, so the computational effort scales linearly with the number of PL.

The layer method has been used mainly to study transport. In 2005 Faleev added an extension to the non-equilibrium case [32]. Because both the crystal and the layer code are based on the Atomic Spheres approximation, they have been mainly applied to transport in magnetic metals that are fairly close packed. It has been extensively used for DFT treatment of spintronic materials; one recent application includes one of the first calculations of spin-orbit torque within DFT [33].

Another novel application is to JMRAM devices where the there are proposals to use stacks of superconducting/ferromagnet/superconducting (SFS) π junctions as components in superconducting circuits [34]. π junctions are built in a manner similar to ordinary MRAM, where the centre region in the diagram above consists of two ferromagnets, separated by a nonmagnetic spacer layer. In ordinary MRAM, the difference in resistance when the two FM layers are aligned ferromagnetically, or antiferromagnetically, forms the basis for the '1' and '0' of a device. A JMRAM devices has much in common with MRAM, but the end leads are superconducting and form Cooper pairs. The Cooper pair undergoes a rotation in the phase when encountering the FM region. In a stack, if the FM regions are aligned parallel, the phase shifts add; when aligned antiferromagnetically, they subtract. Thus the stack can be constructed so the Cooper pair undergoes a phase change of π, or none at all. The change in current-phase relation provides the basis for a binary pair of '1' and '0' states, to make a component of a superconducting circuit.

To model this, the usual Landauer Buttiker description must be augmented by a coupling between the $+k$ and $-k$ states in the leads (Cooper pair), and the Andreev reflection calculated in the presence of the coupling. Working with Microsoft, Herve Ness has successfully built such a description, and is able to describe this phenomenon in a density-functional framework. That the current phase relation should oscillate with FM layer thickness was shown by Buzdin [35], and it has been observed in several materials, e.g. Nb/Co/Nb [34]. Not surprisingly, Ness finds that real band structures greatly modify results Buzdin's simple models, where analytical expressions are derived by assuming free electron bands and small exchange splitting of the ferromagnet [35]. Neither assumption is applicable to real devices. This work will be published elsewhere.

8 Conclusions

Questaal's features were summarised, with a focus on its novelty and work in progress towards a next-generation of electronic structure. A detailed description of Questaal was recently published [1]. In this highlight we emphasised the motivation for quasiparticle self-consistent GW, and why high-fidelity methods of the future will need to evolve away from extensions of density-functional theory. It was also shown that why low-order diagrammatic Green's function methods work very well when spin fluctuations are not strong, but break down in systems with strong spin fluctuations. To address them, we presented an argument to explain why the augmentation of QSGW with DMFT should yield a high-fidelity description for strongly correlated materials, in one-particle and two-particle properties. We also showed some new results for unconventional superconductivity — not normally a feature of an *ab initio* method. We are only developing initial results at this stage, but the signs are very promising. This highlight closed with a summary of Questaal's ability to model transport in a DFT framework, and outlined some new, recent applications of this capability.

References

[1] D. Pashov, S. Acharya, W. R. Lambrecht, J. Jackson, K. D. Belashchenko, A. Chantis, F. Jamet, M. van Schilfgaarde, Questaal: A package of electronic structure methods based on the linear muffin-tin orbital technique, Computer Physics Communications 249 (2020) 107065. doi:10.1016/j.cpc.2019.107065.

[2] P. Liu, B. Kim, X.-Q. Chen, D. D. Sarma, G. Kresse, C. Franchini, Relativistic GW+BSE study of the optical properties of Ruddlesden-Popper iridates, Phys. Rev. Materials 2 (2018) 075003. doi:10.1103/PhysRevMaterials.2.075003.

[3] T. Olsen, K. S. Thygesen, Extending the random-phase approximation for electronic correlation energies: The renormalized adiabatic local density approximation, Phys. Rev. B 86 (2012) 081103. doi:10.1103/PhysRevB.86.081103.

[4] F. Bruneval, T. Rangel, S. M. Hamed, M. Shao, C. Yang, J. B. Neaton, molgw 1: Many-body perturbation theory software for atoms, molecules, and clusters, Computer Physics Communications 208 (2016) 149–161. doi:10.1016/j.cpc.2016.06.019.

[5] S. V. Faleev, M. van Schilfgaarde, T. Kotani, All-Electron Self-Consistent GW Approximation: Application to Si, MnO, and NiO, Phys. Rev. Lett. 93 (2004) 126406. doi:10.1103/PhysRevLett.93.126406.

[6] M. van Schilfgaarde, T. Kotani, S. Faleev, Quasiparticle Self-Consistent GW Theory, Phys. Rev. Lett. 96 (2006) 226402. doi:10.1103/PhysRevLett.96.226402.

[7] T. Kotani, M. van Schilfgaarde, S. V. Faleev, Quasiparticle self-consistent GW method: A basis for the independent-particle approximation, Phys. Rev. B 76 (2007) 165106. doi:10.1103/PhysRevB.76.165106.

[8] M. van Schilfgaarde, T. Kotani, S. V. Faleev, Adequacy of approximations in GW theory, Phys. Rev. B 74 (2006) 245125. doi:10.1103/PhysRevB.74.245125.

[9] F. Bruneval, X. Gonze, Accurate GW self-energies in a plane-wave basis using only a few empty states: Towards large systems, Phys. Rev. B 78 (2008) 085125. doi:10.1103/PhysRevB.78.085125.

[10] P. Umari, G. Stenuit, S. Baroni, Optimal representation of the polarization propagator for large-scale GW calculations, Phys. Rev. B 79 (2009) 201104. doi:10.1103/PhysRevB.79.201104.

[11] J. A. Berger, L. Reining, F. Sottile, Ab initio calculations of electronic excitations: Collapsing spectral sums, Phys. Rev. B 82 (2010) 041103. doi:10.1103/PhysRevB.82.041103.

[12] W. Kang, M. S. Hybertsen, Enhanced static approximation to the electron self-energy operator for efficient calculation of quasiparticle energies, Phys. Rev. B 82 (2010) 195108. doi:10.1103/PhysRevB.82.195108.

[13] J. Deslippe, G. Samsonidze, M. Jain, M. L. Cohen, S. G. Louie, Coulomb-hole summations and energies for GW calculations

with limited number of empty orbitals: A modified static remainder approach, Phys. Rev. B 87 (2013) 165124. doi:10.1103/PhysRevB.87.165124.

[14] T. Kotani, M. van Schilfgaarde, Fusion of the LAPW and LMTO methods: The augmented plane wave plus muffin-tin orbital method, Phys. Rev. B 81 (2010) 125117. doi:10.1103/PhysRevB.81.125117.

[15] O. K. Andersen, O. Jepsen, Explicit, First-Principles Tight-Binding Theory, Phys. Rev. Lett. 53 (1984) 2571–2574. doi:10.1103/PhysRevLett.53.2571.

[16] O. K. Andersen, Linear methods in band theory, Phys. Rev. B 12 (1975) 3060–3083. doi:10.1103/PhysRevB.12.3060.

[17] O. K. Andersen, T. Saha-Dasgupta, R. W. Tank, G. K. C. Arcangeli, O. Jepsen, Electronic Structure and Physical Properties of Solids: The Uses of the LMTO Method, in: H. Dreysse (Ed.), Lecture Notes in Physics, Vol. 535, Springer-Verlag, Berlin, 2000.

[18] T. Kotani, M. van Schilfgaarde, Spin wave dispersion based on the quasiparticle self-consistent GW method: NiO, MnO and -MnAs, Journal of Physics: Condensed Matter 20 (2008) 295214. doi:10.1088/0953-8984/20/29/295214.

[19] S. Laricchia, N. Bonini, M. van Schilfgaarde, Electron-phonon coupling within Quasiparticle Self-consistent GW, in: Bulletin of the American Physical Society, American Physical Society, 2019, p. P22.00011.

[20] L. Sponza, P. Pisanti, A. Vishina, D. Pashov, C. Weber, M. van Schilfgaarde, S. Acharya, J. Vidal, G. Kotliar, Self-energies in itinerant magnets: A focus on Fe and Ni, Phys. Rev. B 95 (2017) 041112. doi:10.1103/PhysRevB.95.041112.

[21] B. Cunningham, M. Grüning, P. Azarhoosh, D. Pashov, M. van Schilfgaarde, Effect of ladder diagrams on optical absorption spectra in a quasiparticle self-consistent GW framework, Physical Review Materials 2 (2018) 034603. doi:10.1103/PhysRevMaterials.2.034603.

[22] S. Acharya, D. Pashov, C. Weber, H. Park, L. Sponza, M. V. Schilfgaarde, Evening out the spin and charge parity to increase T_c in Sr_2RuO_4, Communications Physics 2 (2019) 163. doi:10.1038/s42005-019-0254-1.

[23] C. Weber, S. Acharya, B. Cunningham, M. Grüning, L. Zhang, H. Zhao, Y. Tan, Y. Zhang, C. Zhang, K. S. Acharya, D. Pashov, F. Jamet, M. van Schilfgaarde, Possible phonon-induced electronic bi-stability in VO_2 for ultrafast memory at room temperature, arXiv:1901.08139.

[24] R. M. Crdova-Castro, M. Casavola, M. van Schilfgaarde, A. V. Krasavin, M. A. Green, D. Richards, A. V. Zayats, Anisotropic Plasmonic CuS Nanocrystals as a Natural Electronic Material with Hyperbolic Optical Dispersion, ACS Nano 13 (2019) 6550–6560. doi:10.1021/acsnano.9b00282.

[25] E. Baldini, M. A. Sentef, S. Acharya, T. Brumme, E. Sheveleva, F. Lyzwa, E. Pomjakushina, C. Bernhard, M. van Schilfgaarde, F. Carbone, A. Rubio, C. Weber, Electron-Phonon-Driven Three-Dimensional Metallicity in an Insulating Cuprate, to appear in Proceedings of the National Academy of Sciences. Preprint http://arxiv.org/abs/2001.02624.

[26] M. C. T. D. Müller, S. Blügel, C. Friedrich, Electron-magnon scattering in elementary ferromagnets from first principles: Lifetime broadening and band anomalies, Phys. Rev. B 100 (2019) 045130. doi:10.1103/PhysRevB.100.045130.

[27] Y. Zhang, C. Lane, J. W. Furness, B. Barbiellini, J. P. Perdew, R. S. Markiewicz, A. Bansil, J. Sun, Competing stripe and magnetic phases in the cuprates from first principles, Proc. Nat. Acad. Sci. 117 (2020) 68. doi:10.1073/pnas.1910411116.

[28] J. M. Tomczak, M. van Schilfgaarde, G. Kotliar, Many-Body Effects in Iron Pnictides and Chalcogenides: Nonlocal Versus Dynamic Origin of Effective Masses, Phys. Rev. Lett. 109 (2012) 237010. doi:10.1103/PhysRevLett.109.237010.

[29] J. M. Tomczak, QS GW +DMFT: an electronic structure scheme for the iron pnictides and beyond, Journal of Physics: Conference Series 592 (2015) 012055. doi:10.1088/1742-6596/592/1/012055.

[30] M. Gatti, F. Bruneval, V. Olevano, L. Reining, Understanding Correlations in Vanadium Dioxide from First Principles, Phys. Rev. Lett. 99 (2007) 266402. doi:10.1103/PhysRevLett.99.266402.

[31] A. Liechtenstein, M. Katsnelson, V. Antropov, V. Gubanov, Local spin density functional approach to the theory of exchange interactions in ferromagnetic metals and alloys, J. Magn. Magn. Mater. 67 (1987) 65–74. doi:10.1016/0304-8853(87)90721-9.

[32] S. V. Faleev, F. m. c. Léonard, D. A. Stewart, M. van Schilfgaarde, Ab initio tight-binding LMTO method for nonequilibrium electron transport in nanosystems, Phys. Rev. B 71 (2005) 195422. doi:10.1103/PhysRevB.71.195422.

[33] K. D. Belashchenko, A. A. Kovalev, M. van Schilfgaarde, First-principles calculation of spin-orbit torque in a Co/Pt bilayer, Phys. Rev. Materials 3 (2019) 011401. doi:10.1103/PhysRevMaterials.3.011401.

[34] M. A. Khasawneh, W. P. Pratt, N. O. Birge, Josephson junctions with a synthetic antiferromagnetic interlayer, Phys. Rev. B 80 (2009) 020506. doi:10.1103/PhysRevB.80.020506.

[35] A. I. Buzdin, Proximity effects in superconductor-ferromagnet heterostructures, Rev. Mod. Phys. 77 (2005) 935–976. doi:10.1103/RevModPhys.77.935.